CFD of Multiphase Flow in Packed-Bed Reactors: II. Results and Applications

Y. Jiang, M. R. Khadilkar, M. H. Al-Dahhan, and M. P. Dudukovic
Chemical Reaction Engineering Laboratory (CREL), Dept. of Chemical Engineering,
Washington University, St. Louis, MO 63130

Numerical simulations of multiphase flow using the k-fluid CFD model described in Part I of this issue are presented for packed beds at various operating conditions. Both steady-state and unsteady-state (e.g., periodic operation) feed conditions were studied numerically. Predictions of the k-fluid CFD model are comparable with the experimental data in the literature for liquid upflow in a cylindrical packed bed. In addition to the mean porosity and the longitudinally averaged radial porosity profile, the variance of the porosity distribution is needed for predicting the probability density function of the sectional flow velocity. In the trickling flow regime, the k-fluid CFD model provides reasonable predictions of the global liquid saturation and the pressure gradient. Relevant applications of the k-fluid CFD model are identified in quantifying the relationship between bed structure and flow distribution in various-scale packed beds. The combined flow-reaction modeling scheme is proposed through the "mixing-cell" network concept, in which the k-fluid CFD simulation can provide the information on sectional flow distribution.

Introduction

In recent years, computational fluid dynamics (CFD) has become an important tool in studies of multiphase flows. It is expected that CFD modeling will become more pervasive in the design of multiphase reactors as researchers in both academic and industrial communities are intensifying their efforts in this area. So far the CFD approach has been used to simulate single-phase and multiphase flow within relatively simple geometries and to compare the results to those obtained from experiments (Kuipers and van Swaaij, 1998; Lahey and Drew, 1999; Pan et al., 2000). More complex systems, such as multiphase flows in packed beds, have not been studied in detail by the CFD approach due to the complex geometry of the tortuous pore space and the complicated fluid–fluid and fluid–particle interactions. A new strategy for flow modeling in packed beds is devised by implementing the statistical description of the bed structure into the CFD model and by using the drag forces that have been developed and discussed in Part I (Jiang et al., 2002). A multidimensional *k*-fluid Eulerian model has been adopted and executed in the framework of the CFDLIB package from Los Alamos National Laboratory. The details of this code are available elsewhere (Kashiwa et al., 1994; Johnson, 1996; Johnson et al., 1997).

Since the void space and the flow distribution in random packed beds are intrinsically statistical in nature, a statistical approach to porosity distribution description in the bed certainly has an advantage over the conventional deterministic assignment of mean porosity everywhere in the bed and/or the use of longitudinal-averaged radial porosity profile (Stanek, 1994; Bey and Eigenberger, 1997; Yin et al., 2000). Up to now, there have been few comparisons between the CFD results and the measured flow data in the bed with randomly packed particles, such as the upflow studies with different liquids of Stephenson and Stewart (1986). These comparisons, however, were limited to the use of longitudinally averaged radial velocity profiles at different particle Reynolds numbers ($Re_p = 5,\ 80$), and no statistical quantities [e.g., probability density function (p.d.f.)] of the two-dimensional velocity field were reported (Jiang et al., 2000). In this article, we expand the preceding study to include the comparison of the probability density function of the sectional liquid-velocity distribution.

The entrance (or feed) distribution of fluid(s) is controlled by the distributor design and the top layer of the packing.

Correspondence concerning this article should be addressed to M. P. Dudukovic.
Present addresses of: Y. Jiang, Conoco Inc., 1000 South Pine St., Ponca City, OK 74602; M. R. Khadilkar, GE Plastics, 1 Lexan Lane, Mt. Vernon, IN 47620.

The effects of the feed distribution on the macroscopic flow structure were found significant in the experiments (Christensen et al., 1986; Szady and Sundaresan, 1991) and in the numerical simulations (Anderson and Sapre, 1991; Jiang et al., 1999). The use of inert large particles as the top layer is rather common in commercial packed columns. In fact, Moller et al. (1996) found that compact ceramic cylindrical tablets, TK-10, on the top of packed beds of 1/16-in. cylindrical extrudates have a positive effect on the liquid distribution (such as the top layer compensates for the poor inlet distribution). However, a negative effect on liquid distribution (such as enhancing rivulet flow) was reported by Szady and Sundaresan (1991) in the packed bed of 3-mm glass spheres topped with a 10-cm layer of 6-mm Rashig rings. The discrepancy in the effect of the top layer might be due to the different particle structures used in the two studies for the top layer, which provide a different number of rivulets of the liquid, but definitely the flow distribution is sensitive to the upper boundary of flow, particularly in the trickling flow regime (Szady and Sundaresan, 1991). Any uneven feed distribution due to the distributor or the top layer can cause a change in the downstream flow pattern. In this article, we intend to explore such flow phenomena numerically by computing the flow pattern based on the *k*-fluid CFD model.

A designed dynamic flow modulation of the inlet fluid has been demonstrated to achieve reactor performance better than that attainable in steady-state operation for α-methylstyrene hydrogenation (Khadilkar et al., 1999) and in SO_2 oxidation (Silveston, 1990). The evidence of any improvement of the flow distribution under dynamic inflow modulation has not been reported in open literature. The unavailability of the related flow distribution data might be due to the difficulty with the needed flow measurements. Therefore, the adopted *k*-fluid model, which is capable of dynamic flow simulation, allows us to perform numerical flow simulations under such inflow modulation, which can then provide a quantitative comparison of the flow distribution under steady-state and unsteady cyclic mode of operation. Such modeling results can provide rational explanations for the performance enhancements observed in the experimental studies.

Several unresolved issues regarding flow maldistribution still remain in scaling up a bench-scale packed-bed and in scaling down a commercial unit to mimic its performance in a laboratory scale bed. In many cases, the scaling down of multiphase packed beds is even tougher, since many issues, such as liquid back mixing, liquid maldistribution, and "wall effects," become more apparent when the reactor scale is reduced (Mears, 1971; Tasmatsoulis and Papayannakos, 1994; Sie and Krishna, 1998). The adopted CFD model is used to help develop the understanding of multiphase flow phenomena in bench-scale packed beds and to interpret some unusual experimental results encountered in hydrodynamic and mass-transfer measurements. The CFD model also ought to help us understand the structure–flow relation in packed beds and the role of the operating conditions and scale-up on such relations.

The final goal of this long-term project is to establish an advanced modeling strategy for packed-bed reactors, which will not only provide a means for new reactor design but will also serve well as a diagnostic tool for the operating units. For this reason, the coupling of the flow information obtained from CFD with chemical kinetics to predict the reactor performance becomes an essential step. In this article, the previous cell-network approach (Deans and Lapidus, 1960) has been adopted in a novel way in which the disadvantages of previous cell models have been overcome to a large extent. A combination of CFD flow modeling and mixing-cell reactor modeling is suggested as an efficient alternative for modeling multiphase flow with complex chemistry in packed-bed reactors.

This article has been organized in the following manner. First, we present a comparison of CFD predictions and experimental data for liquid upflow in packed beds. Then, we report some comparisons of CFD computations and the measured liquid holdup and pressure-drop in a pilot-scale trickle bed with gas and liquid cocurrent downflow. We report only global quantities due to the lack of data on the spatial distribution of these quantities. The third part presents some simulation results regarding the effects of feed distribution, at steady-state and unsteady-state conditions, on the downstream flow distribution. In the fourth part, we discuss some applications of the developed *k*-fluid CFD model in the scale-up and scale-down as well as in coupling with kinetics.

Comparison of CFD Simulation and Experimental Results

Since the CFD approach to flow modeling presented in Part I (Jiang et al., 2002) has to be based on known porosity distribution at a certain scale, a full-comparison of CFD predictions and experimental data are possible *only if* the data for distribution of porosity, velocity, and phase volume-fraction are available on the same scale. The lack of such sets of experimental data in packed beds has made the full validation of the current CFD model impossible. Magnetic resonance imaging (MRI) has recently shown some promise in providing phase holdup and velocity distribution data in packed beds (Sederman et al., 1997), and it has been utilized for the validation of lattice-Boltzmann simulation for single-phase flow (Manz et al., 1999). For the multiphase flow of interest in this work, there are no suitable data in the open literature. What we found in the literature so far are only a few experimental results that could be used only for partial validation of our CFD simulation results. For example, Stephenson and Stewart (1986) presented the longitudinally averaged radial profile of porosity in a packed bed of spheres and the corresponding liquid upflow velocity profiles obtained from cylindrical packed beds using a *marker tracking* method (that is, optical measurement). Data are provided for several particle Reynolds numbers within the range from 5 to 280 in the beds with $D_r/d_p = 10.7$ and $L/d_p = 20.6$. The statistical information, such as the histogram of the axial interstitial velocity distribution, was also reported in the article. In at least a partial validation of the numerical CFD results, we reported (Jiang et al., 2000) the comparison of the CFD predicted velocity profiles and the measured profiles of Stephenson and Stewart (1986) at particle Reynolds numbers of 5 and 80 for the liquid upflow case. For a multiphase flow system, such as gas–liquid flow in a packed bed, there are no suitable data for a similar comparison. What we can do is to look at the CFD predictions of the global hydrodynamic quantities, such as overall liquid holdup and pressure gradi-

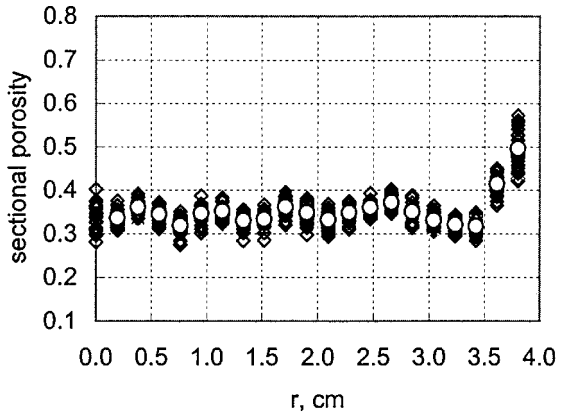

Figure 1a. Generated sectional porosities (RN1) plotted as a function of radial position (◇) and longitudinally averaged radial porosity profile of Stephenson and Stewart (1986) (○).

Statistics of the RN1 distribution (mean and standard deviation) are given in Table 1.

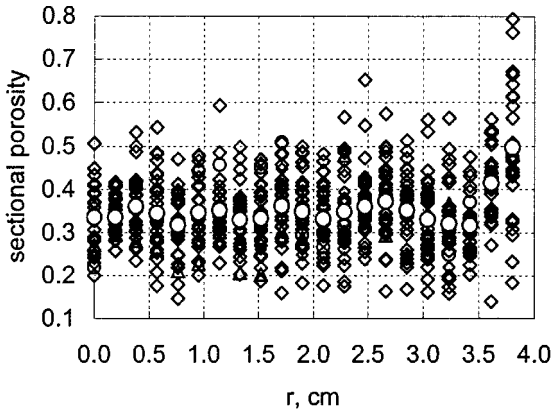

Figure 1b. Generated sectional porosities (RN2) plotted as a function of radial position (◇) and longitudinally averaged radial porosity profile of Stephenson and Stewart (1986) (○).

Statistics of the RN2 distribution (mean and standard deviation) are given in Table 1.

ent, and compare these quantities quantitatively with the experimental data. For the predicted distributed quantities, a qualitative comparison is the only choice, as the data for the distribution of porosity, multiphase velocities, and phase volume fraction are available only based on the computational results obtained at different conditions.

Liquid upflow in packed beds

Because of the lack of the two-dimensional (2-D) measured porosity distribution data in the article by Stephenson and Stewart (1986), the comparison of CFD predictions for liquid upflow in packed beds was limited to the longitudinally averaged radial profiles of axial velocity, in which only the one-dimensional (i.e., radial) variation of porosity was implemented in the CFD flow simulation. That means there was no axial porosity variation at each radial position [that is, $\epsilon(r,z) = \epsilon(r)$] in the previous flow simulations. Although the simulated longitudinally averaged radial velocity profiles agree well with the experimental data, as shown in Jiang et al. (2000), the probability density function (p.d.f.) of the axial interstitial velocity component (V_z) from the CFD flow simulations could not be compared with the p.d.f. data reported in Stephenson and Stewart (1986). Clearly, there is a need to use a 2-D variation in the sectional porosity assignment [$\epsilon(r,z)$] in the CFD flow simulation in order to achieve a comparable p.d.f. for sectional velocity components.

In the absence of experimental data on the distribution of porosity to the level of detail needed for CFD, a statistical approach has to be employed to generate the local values while keeping global averages identical to experimental values. Continuing the discussion initiated in Part I (Jiang et al., 2002), a packed bed can be treated as a network of interconnected sections with a certain section size (see Figure 2 in Part I). The macroscale sectional porosities are normally distributed in a pseudo-Gaussian manner, except when the section size is extremely small, and then a pseudobinomial distribution might be expected. In this study, based on the mean porosity and the reported longitudinally averaged radial porosity profiles with two different standard deviations, we generated two sets of pseudo-Gaussian porosity distributions, namely, RN1 and RN2. The sectional porosities together with the longitudinally averaged porosity values from Stephenson and Stewart (1986) are plotted in 2-D cylindrical coordinates (r,z), as shown in Figures 1a and 1b. The heterogeneity of the RN2 bed is clearly higher than that of the RN1 bed, as one can see from the standard deviations of the two porosity distributions in Table 1. Figure 2a shows the comparison of the predicted and the measured longitudinally averaged radial profiles of the axial velocity component for the RN1 porosity assignment at different Reynolds numbers. The experimental data shown in Figure 2a are based on the averaged result at different Reynolds numbers (see Stephenson and Stewart, 1986). Similarly, Figure 2b gives the comparison

Table 1. Statistical Description of Porosities and CFD Simulated Velocities

Two Random Packed Beds	RN1	RN2
Porosity	Mean = 0.3527 Std = 0.0420	Mean = 0.3534 Std = 0.0916
Axial interstitial velocity, V_z, cm/s		
Std/mean ($Re = 5$)	2.0012/6.6740	3.8640/7.0915
Std/mean ($Re = 280$)	6.9313/29.8377	12.0708/31.3548
Radial interstitial velocity, V_x, cm/s		
Std/mean ($Re = 5$)	0.4379/0.1029	1.8790/(−0.2034)
Std/mean ($Re = 280$)	1.2752/0.2645	7.7352/(−1.5758)

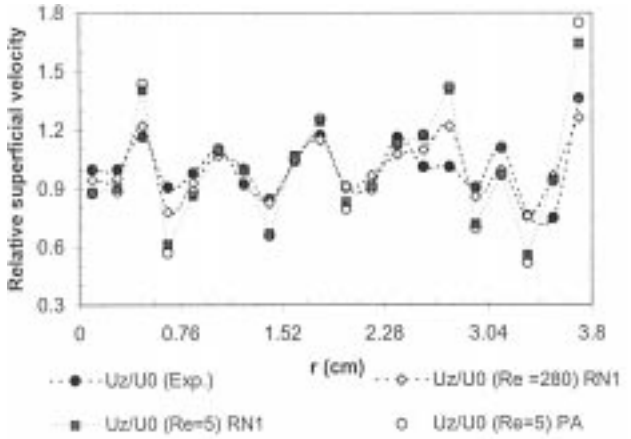

Figure 2a. Longitudinally averaged radial profiles of axial velocity at different Reynolds numbers vs. experimental data of Stephenson and Stewart (1986).

Statistics of the RN1 bed (i.e., mean and standard deviation) are available in Table 1; parallel bed (PA): sectional porosities are only varying in the radial direction.

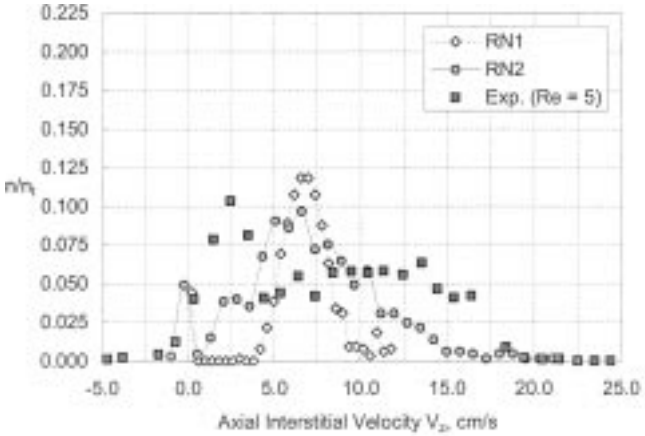

Figure 3a. Frequency distribution of axial interstitial velocity ($Re = 5$).

RN1-CFD simulation based on random porosity set 1; RN2-CFD simulation based on random porosity set 2; Exp.—experimental data reported by Stephenson and Stewart (1986).

for the RN2 porosity assignment case. From this it follows that the longitudinally averaged radial profile of the axial velocity component can be well predicted by the *k*-fluid CFD model provided that the longitudinally averaged radial profiles of sectional porosity are implemented in the simulation. This is expected since the longitudinally averaged radial porosity profile determines the longitudinally averaged velocity profile. However, significant differences do exist in the predicted statistical information of the sectional liquid velocities based on two different porosity distributions RN1 and RN2 in the beds. As one can see from Figures 3a and 3b, the histogram of the predicted liquid axial velocity in the RN2 bed is much closer to the experimental data than that in the RN1 bed. This implies that the sectional porosities in the experimental beds are much more spread than a narrow Gaussian distribution and are much closer to the RN2 bed shown in Figure 1b. This is most likely caused by the fact that cylindrical particles were used in the experiments of Stephenson and Steward (1986), and larger spread in the porosity distribution is expected with cylindrical particles than with spherical particles (Bey and Eigenberger, 1997). This indicates that if we know the mean porosity, the longitudinally averaged radial porosity profile, and the variance of sectional porosity distribution, we can predict the variance of the sectional velocity distribution. In fact, our CFD simulations have found that if we fix the mean porosity, the longitudinally averaged porosity profile, and the variance of the sectional porosity distribution, we can achieve the same variance of the flow

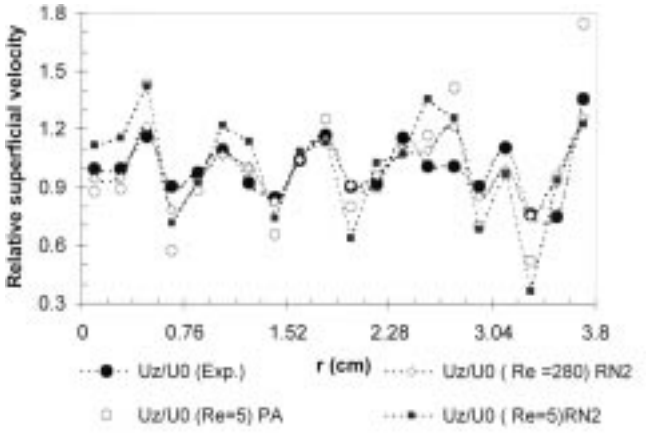

Figure 2b. Longitudinally averaged radial profiles of axial velocity at different Reynolds numbers vs. experimental data of Stephenson and Stewart (1986).

Statistics of the RN2 bed (i.e., mean and standard deviation) are available in Table 1; parallel bed (PA): sectional porosities are only varying in the radial direction.

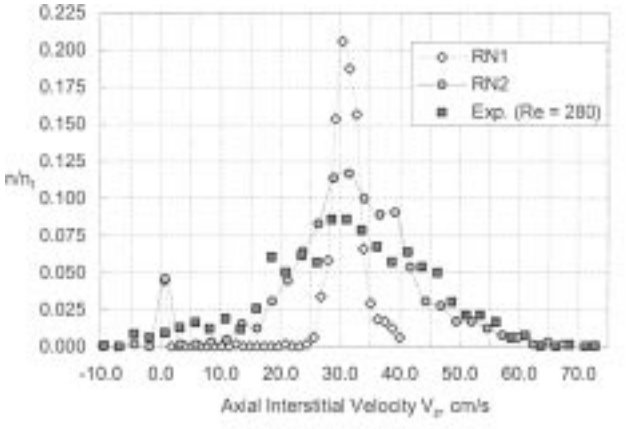

Figure 3b. Frequency distribution of axial interstitial velocity ($Re = 280$).

RN1-CFD simulation based on random porosity 1 (ϵ: std/μ = 0.0916/0.3534; V_x: std/μ = 1.879/0.2034; V_z: std/μ = 3.864/7.0915); RN2-CFD simulation based on random porosity 2 (ϵ: stu/μ = 0.0916/0.3534; V_x: std/μ = 1.879/0.2034; V_z: std/μ = 3.864/7.0915); Exp.—experimental data reported by Stephenson and Stewart (1986).

velocity even if we have different porosity assignments in the flow simulations.

Based on the preceding simulations, for single phase flow, we conclude that the *k*-fluid model can predict not only the longitudinally averaged radial profiles of axial velocity but also can provide the statistical information (p.d.f.) on the fluid velocity distribution provided that the following information on bed structure is *all* available:

1. Mean porosity;
2. Longitudinally averaged radial porosity;
3. Sectional porosity distribution type and its variance.

The mean porosity and the longitudinally averaged radial porosity profile are obtainable by experiments and are also predictable by various empirical correlations in the literature (Benenati and Brosilow, 1962; Muller, 1991; Bey and Eigenberger, 1997). The p.d.f. of the porosity distribution is a function of particle size, shape, column diameter, as well as the packing method, which can, in principle, be developed through 3-D packing computer simulations (see Tory et al., 1973) and extensive MRI measurements of packed-bed structures (see Baldwin et al., 1996; Sederman et al., 1997).

Gas and liquid cocurrent downflow in trickle beds

One should note that the preceding comparisons are limited to a system that consists of a fixed solid phase which is saturated with a flowing fluid, typical examples of which are (1) gas flowing through fixed beds; (2) and liquid upflow through packed beds (Stephenson and Stewart, 1986). For packed beds with gas and liquid two-phase flows (such as gas–liquid cocurrent downflow in trickle beds), the competition of gas and liquid for the fixed cavities between solid particles makes the liquid distribution much more complicated than the saturated single-phase flow distribution. In this subsection, we intend to partially validate the CFD two-phase flow predictions by comparing them with the experimental data for overall liquid saturation and overall pressure gradient. The case of two-phase flow in a pilot-scale trickle bed with relatively high gas superficial velocity (e.g., 0.22 m/s) is chosen to assess the model capability in scaling up trickle-bed reactors. The simulations were based on a cylindrical column having an internal diameter (ID) of 0.152 m. The packing part is 1.50 m high and consists of 3 mm spherical particles. The measured voidage of $\backsim 0.37$ was used as the mean porosity. The working fluids were air for the gas phase and water for the liquid phase. The experimental data were obtained from the article by Szady and Sundaresan (1991), in which the overall liquid saturation and pressure gradient data were reported in packed beds with similar dimensions in both trickling and pulsing flow regimes.

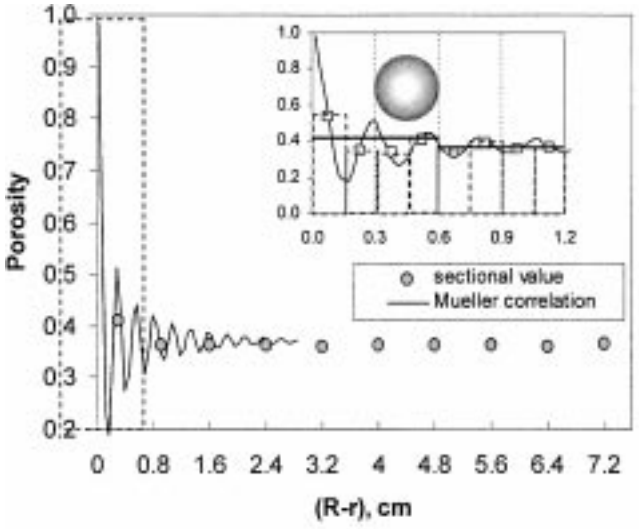

Figure 4a. Discretization of the radial porosity profile into sectional porosity values ($d_p = 3$ mm).

From the wall to the center: sectional mean = 0.411, 0.363, 0.363, 0.365, 0.362, 0.362, 0.363, 0.364, 0.362, 0.366; sectional std/mean = 20%, 15%, 10%, 10%, 10%, 10%, 10%, 10%, 10%, 10%.

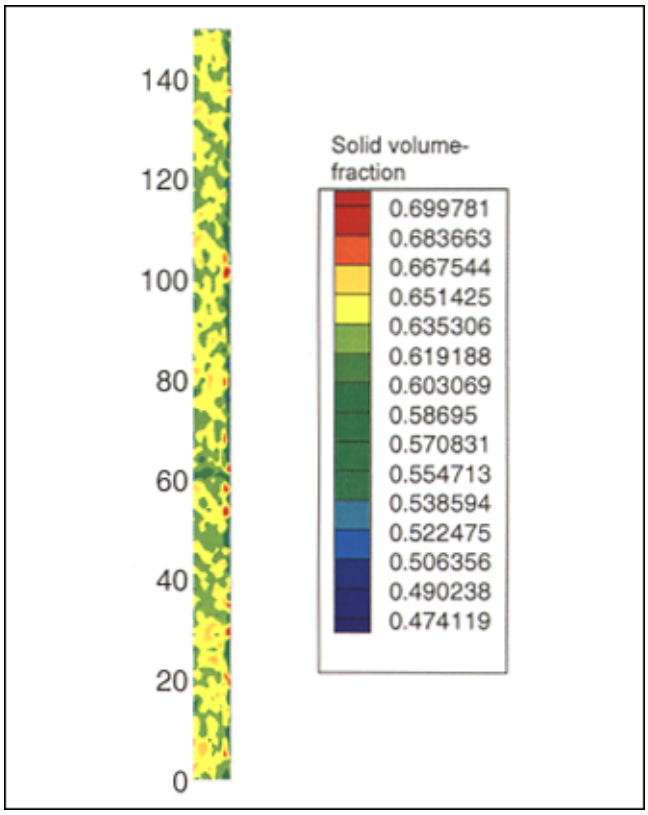

Figure 4b. Solid volume-fraction distribution generated based on the data in Table 2 in a pilot scale packed bed.

Before computing the two-phase flow using the *k*-fluid CFD model, one needs to generate a multidimensional porosity distribution at a certain sectional size, as discussed in Part I. For an axisymmetric cylindrical column, a two-dimensional porosity distribution, $\epsilon(r,z)$, is needed for flow simulation. Based on the measured mean porosity and the longitudinally averaged radial porosity profile curve calculated by Mueller's (1991) model, one can discretize the radius, r, into several annular sections, and calculate the sectional porosities by integrating the radial porosity profile curve as shown in Figure 4a. It is known that the oscillation of the porosity profile is pronounced in the wall zone, which is about 3–4 particle di-

Table 2. Parameters Used in Discretization of Radial Porosity Profile and Generation of 2-D Porosity Distribution

Two Regions	Wall	Core
Section no. and size in r	2, 0.6 cm	8, 0.8 cm
Section no. and size in z	150, 1 cm	150, 1 cm
Radial position (from center to wall), cm	7.6, 7.0	6.4, 5.6, 4.8, 4.0, 3.2, 2.4, 1.6, 0.8
Longitudlnal-avgd. Sectional porosity	0.411, 0.363	0.363, 0.365, 0.362, 0.362, 0.363, 0.364, 0.362, 0.366
Ratio of std./mean	0.2, 0.15	0.1, 0.1, 0.1, 0.1, 0.1, 0.1, 0.1, 0.1, 0.1

ameters from the wall. The variance of porosities in the wall region is expected to be higher than that in the core region. Table 2 lists the parameters used in the discretization of the annular sections, and Figure 4b displays the solid volume-fraction distribution of the generated packed bed, in which the porosities of 1,500 ($=10\times150$) sections are represented by a 2-D pseudo-Gaussian distribution, with the standard deviations given in Table 2. There are two annular sections in the radial direction (r) in the wall region with relatively small section size. The section size in longitudinal direction (z) is 0.01 m. At the top boundary of the bed, it was assumed that a uniform gas and liquid feed distribution is attained as claimed in the experiments (Szady and Sundaresan, 1991). Figures 5a and 5b show the simulated liquid and gas volume-fraction distribution at a gas superficial velocity of 0.22 m/s and liquid superficial velocity of 0.0045 m/s. Relatively high liquid and gas holdups appear in the wall region where the porosities are high due to the wall interference.

In Figures 6 and 7, we compare the CFD predictions of the overall liquid saturation and pressure gradient with the experimental data of Szady and Sundaresan (1991) at different liquid superficial velocities. We also plotted the calculated values from the single-slit model (Holub et al., 1992) and the relative permeability model (Saez and Carbonell, 1985). As discussed in Part I, there is a need to predetermine the values of the two Ergun constants (E_1 and E_2) experimentally when using Holub's model to calculate the overall liquid holdup and pressure drop. Similarly, the static liquid holdup, ϵ_L^0, has to be determined in order to calculate ϵ_L and $(\Delta P/\Delta z)$ in Saez and Carbonell's model. The predictions obtained by Holub's model shown in Figures 6 and 7 are based on the measured values, $E_1 = 215$ and $E_2 = 1.4$. Two sets of calculated results from the Saez and Carbonell model are also plotted in Figures 6 and 7. One set of data is based on the

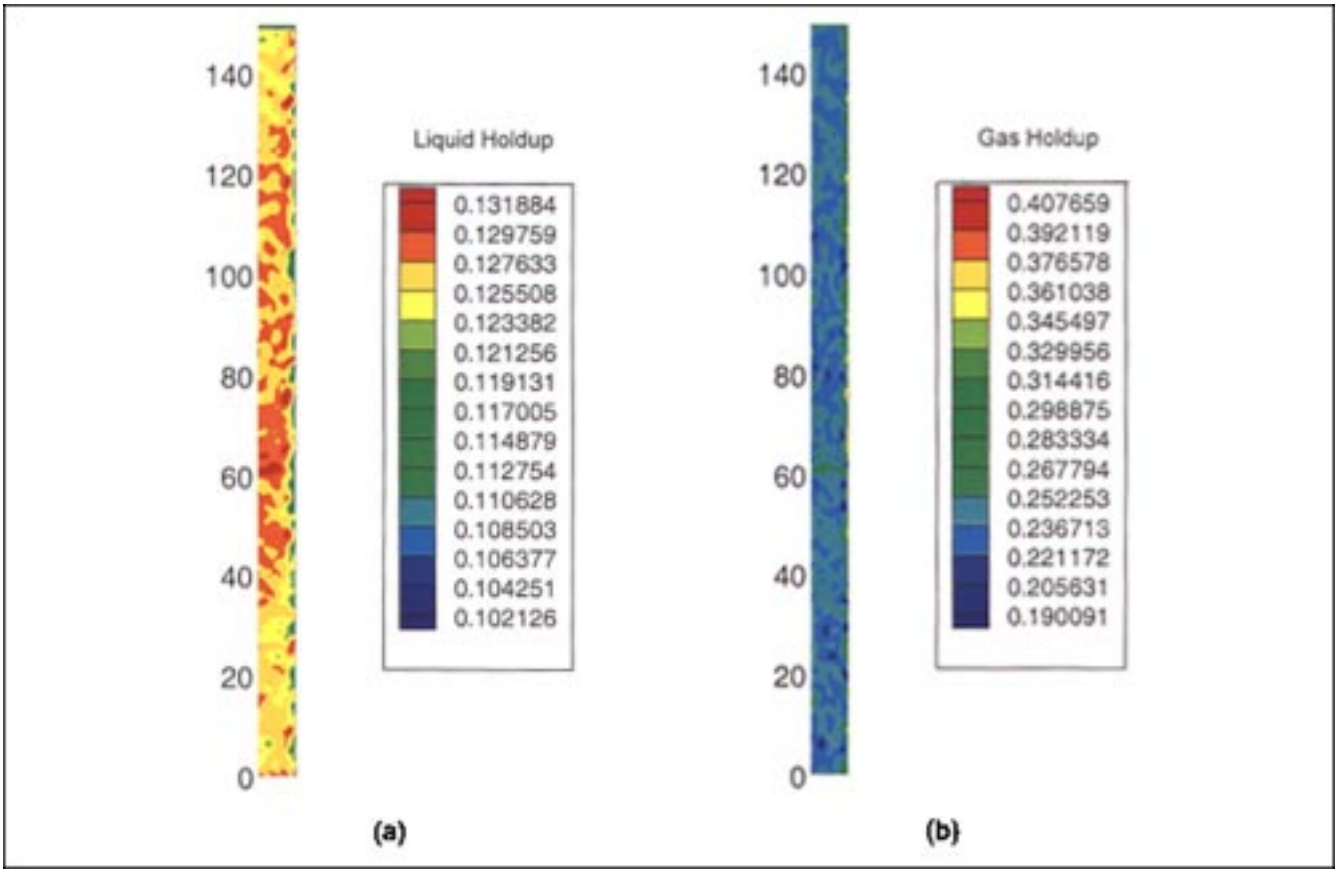

Figure 5. Simulated phase volume-fraction distribution at liquid superficial velocity of 0.45 cm/s and gas superficial velocity of 22 cm/s in a pilot-scale packed bed: (a) liquid; (b) gas.

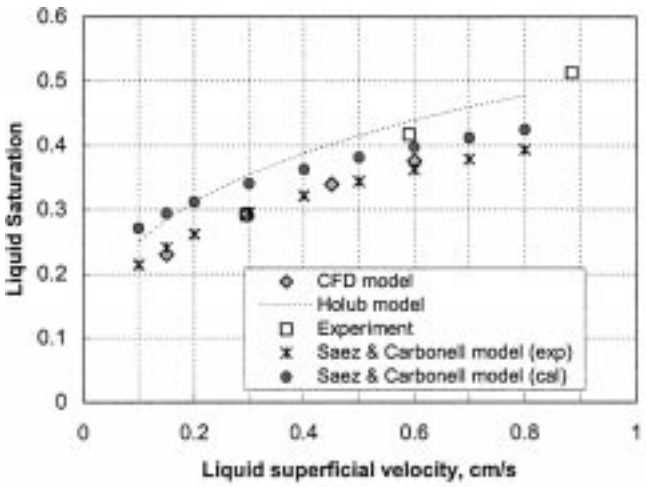

Figure 6. CFD *k*-fluid model prediction of liquid saturation vs. experimental data of Szady and Sundaresan (1991) (gas superficial velocity is 22 cm/s) and other models.

The f values used in CFD modeling are evaluated by the external particle wetting efficiency correlation by Al-Dahhan and Dudukovic (1995). Exp.—Use measured static liquid holdup (0.022) in Saez and Carbonell model; cal—use the correlation-estimated value (0.05) in Saez and Carbonell model.

measured static liquid holdup ($\epsilon_L^0 = 0.022$) (marked as "exp"), the other set of data is based on the correlation-estimated value ($\epsilon_L^0 = 0.05$) (marked as "cal"). The mean values for liquid saturation and pressure gradient from the *k*-fluid CFD model are plotted together with these data. In the *k*-fluid CFD simulations, the momentum exchange coefficients, X_{gs} and X_{ls}, are calculated from the Holub formula with two Ergun constants E_1 ($=180$) and E_2 ($=1.8$), and X_{gl} is from Attou et al. (1999). A detailed discussion of X_{kl} calculations was provided in Part I (Jiang et al., 2002). It should be noted that the use of Ergun constants, E_1 and E_2, determined with single-phase flow in the packing of interest, is employed in some two-phase flow models (e.g., Holub et al., 1992) precisely for the purposes of accounting for the voidage distribution effect in the bed on the fluid–solid drag, as mean voidage for the bed is used in these equations. In our CFD model, however, we feel justified in using the standard values of the E_1 and E_2 constants for drag modeling at the cell level, because the voidage effect is directly incorporated via the voidage distribution. Hence, if the drag relationship was represented at the bed level based on mean voidage, modified values of E_1 and E_2 may be observed.

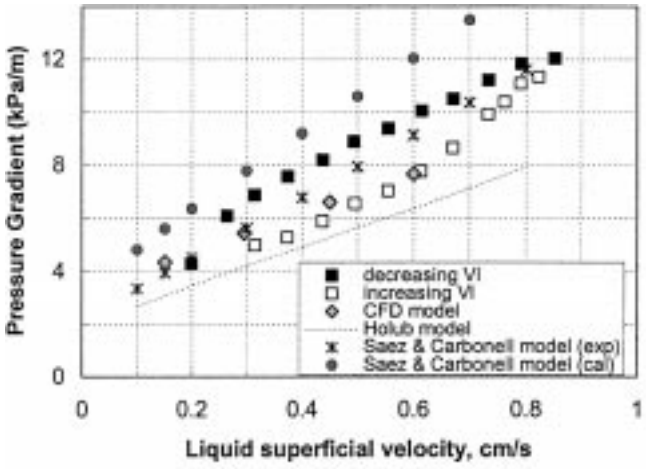

Figure 7. CFD *k*-fluid model and phenomenological models prediction of pressure gradient vs. experimental data of Szady and Sundaresan (1991) (gas superficial velocity is 22 cm/s).

The f values used in CFD modeling are evaluated by the particle external wetting efficiency correlation by Al-Dahhan and Dudukovic (1995). Exp—use measured static liquid holdup (0.022) in Saez and Carbonell model; cal—use the correlation-estimated static liquid holdup (0.05) in Saez and Carbonell model.

Both bed-scale models (Holub model and Saez and Carbonell model with calculated ϵ_L^0) give unsatisfactory predictions of the pressure gradient. The *k*-fluid CFD model and Saez and Carbonell's model with measured ϵ_L^0 provide a more reasonable prediction for the pressure gradient and a better prediction for liquid saturation, as one can see from Figures 6 and 7. Comparison of the *k*-fluid CFD model predictions with additional experimental data on overall liquid holdup and the pressure gradient can be performed in the future to fully assess the utility of the *k*-fluid CFD model in predicting the overall hydrodynamic quantities. The onset of the natural pulsing was experimentally observed at the liquid superficial velocity of 0.8 cm/s at the given gas superficial velocity of 22 cm/s. It seems reasonable that the *k*-fluid CFD model should produce agreeable predictions of the overall hydrodynamics quantities in the trickling-flow regime (e.g., liquid superficial mass velocity < 6 kg/m^2/s), for which proper closures were provided. As we discussed in Part I, the interactions between the fluid and particles, fluid and fluid become very complicated at the flow transition regime and in the pulsing flow regimes that remain a challenge for researchers (Szady and Sundaresan, 1991).

One should note that the superiority of the *k*-fluid CFD model to other phenomenological hydrodynamic models can be attributed to its ability to provide not only the global hydrodynamics quantities such as liquid holdup and pressure drop but also the spatial distribution information on hydrodynamic quantities in multidimensional packed beds.

Simulation of Feed Distribution Effects

There have been many discussions about the role of feed distribution on flow distribution inside packed beds in the literature, particularly for gas–liquid cocurrent downflow in the trickling-flow regime where well-designed gas and liquid distributors are important for achieving good flow distribution. Beyond this general concern, however, there have been some discrepancies reported on how the feeding of the liquid and gas affects the downstream flow pattern, particularly in the quantitative sense. In fact, there are many parameters that contribute to the feed distribution effect. In most absorption columns, packed with relatively large elements ($\backsim$ 2–10 cm), the inertial force and gravity play an important role in causing significant wall flow, but the particle wetting seems not to be a significant factor for large-size packing (Stanek, 1994). However, in most trickle beds with relatively

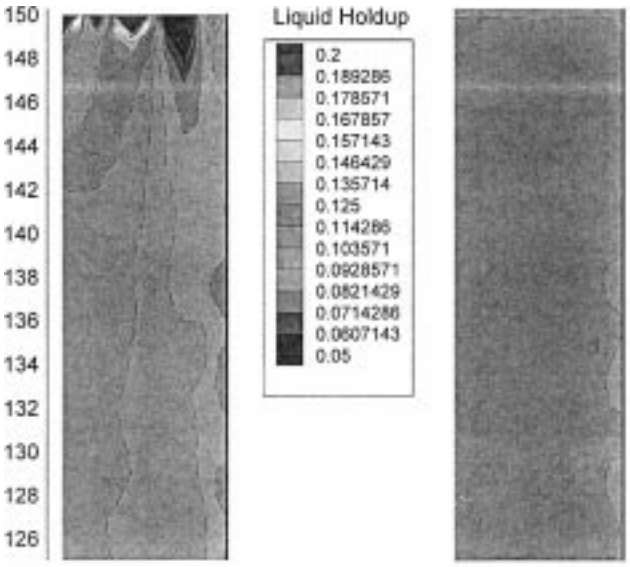

Figure 8a. Liquid-holdup distribution under: nonuniform (left) vs. uniform (right) feed conditions at $U_{l0} = 0.295$ cm/s, $U_{g0} = 22$ cm/s.

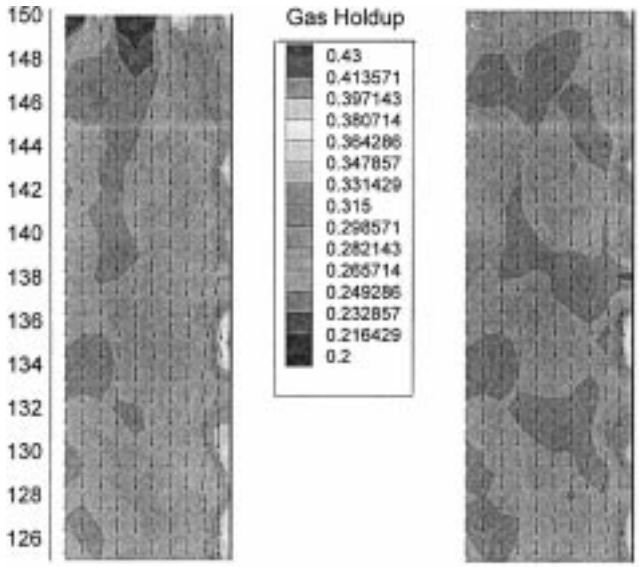

Figure 8b. Gas-holdup contour and gas interstitial velocity vector plot under: nonuniform (left) vs. uniform (right) feed conditions at $U_{l0} = 0.295$ cm/s, $U_{g0} = 22$ cm/s.

small porous particles (~ 0.5–5.0 mm), the capillary force and particle partial external wetting become important in determining the flow distribution so that significant feed distribution effects on flow and wetting were found (Jiang et al., 1999).

Unsteady-state feed distribution has been proposed as a means to intensify the process performance by improving the yield of the desired product at the same time-averaged flow rate as used at steady state. This is the so-called "periodic flow operation" or "induced pulsing operation" (Haure et al., 1989; Tsochatzidis and Karabelas, 1995). The enlarged pulsing flow regime, favored in most commercial units, has been experimentally found under such an operating mode (Boelhouwer et al., 2001). Although experimental evidence for performance enhancement has been reported, the explanation for this improvement has not focused on the possible improvements in flow distribution. Moreover, it is also quite difficult to accurately measure the difference in liquid distribution using the conventional exit-flow measurement at steady state at induced pulsing operations (Jiang, 2000). To measure unsteady-state flow distribution in such a pulsing flow, even with MRI or computer tomography (CT), remains a challenge due to both the high spatial and temporal resolutions that are required. As a preliminary study of this topic, we provide a set of numerical results that describe the simulated flow distribution under steady-state operation mode and its improvement by induced liquid pulsing operation mode.

Steady-state liquid input

Three types of liquid inlet distributors: single-point source, two-point source, and uniform distributor have been tested in numerical simulations using the discrete cell model (DCM) approach based on the minimization of the total energy dissipation rate in packed beds (Jiang et al., 1999). The effect of liquid feed distribution was observed to be significant in the upper half of the bed, and less pronounced at depths exceeding 50 particle diameters (15 cm) for a total bed length of 96 particle diameters. Since the steady-state simulations of Jiang et al. (1999) were limited to a bench-scale 2-D rectangular packed bed, it is desirable to see if those effects are retained in a cylindrical pilot-scale packed bed. Hence, we test the effect of a nonuniform steady-state liquid feed distribution in the pilot-scale trickle bed used earlier (see Figures 8a and 8b) on the downstream two-phase flow distribution using the CFD *k*-fluid simulation. The averaged feed superficial velocity for the top ten sections is 0.295 cm/s for liquid and 22 cm/s for gas. Table 3 lists the sectional velocities and volume-fractions of the ten top layer sections for flow simulation with a nonuniform feed distribution. Such uneven liquid feed distribution might result from the improper design of the liquid distributor or be due to the improper use of the top-layer of packing.

The gas- and liquid-flow maldistribution are detected at downstream locations for a nonuniform gas and liquid feed

Table 3. Feed Velocities and Holdup at Top Ten Sections from Center to Wall

Section	1	2	3	4	5	6	7	8	9	10
U_l (cm/s)	0.885	0	0	0.738	0.738	0	0	0	0.295	0.295
ϵ_l	0.363	0	0	0.373	0.391	0	0	0	0.150	0.100
U_g (cm/s)	0	33.0	33.0	0	0	36.67	36.67	36.67	22.0	22.0
ϵ_g	0	0.389	0.362	0	0	0.360	0.370	0.364	0.218	0.397

distribution, listed in Table 3, and show that the overall liquid holdup decreases by ~11% (from 0.1084 for uniform inlet to 0.0968 for nonuniform inlet). Moreover, the maldistribution is more significant in the upper 25-cm portion of the packed bed, although the effect does propagate throughout the whole packed bed. Figure 8a exhibits the comparison of the liquid holdup distribution at nonuniform feed condition (left plot) and uniform feed condition (right plot). Figure 8b displays the gas holdup contour plot and gas interstitial velocity plot at the nonuniform and uniform feed condition. At high gas superficial velocity, more gas flow is encountered in the wall region due to the higher porosity, as shown in Figure 8b (right plot). The nonuniform feed of gas and liquid make the gas maldistribution worse, as one can see from Figure 8b (left plot).

Periodic liquid input

A test case with a possibility of significant liquid maldistribution was chosen for investigating the effects of induced liquid flow modulation. A 2-D bench-scale rectangular model bed of dimensions 29.7 cm × 7.2 cm was considered with preassigned porosity values to different sections (33 in the vertical (Z) direction and 8 in the horizontal (X) direction). Thus 264 values of porosity were generated (with the mean porosity of 0.406 and a variance of 0.04) to form a pseudorandom pattern of porosities in the bed (as shown in Figure 9). Liquid flow was introduced at the two central cells at the top of the bed at a mean interstitial velocity of 0.1 cm/s, while gas flow was introduced in the rest of the cells at an interstitial velocity of 10.0 cm/s in simulations of both steady- and unsteady-state operation. Steady-state simulation shows evidence of significant liquid maldistribution, particularly at the top and bottom of the reactor (Figure 10). The complete absence of liquid is seen in zones near the bottom of the reactor (Figure 10). Some spreading effect is seen as shown in the steady-state study, but is not sufficient to overcome the inherent maldistribution effects due to central liquid inlet and the porosity profile in the bed.

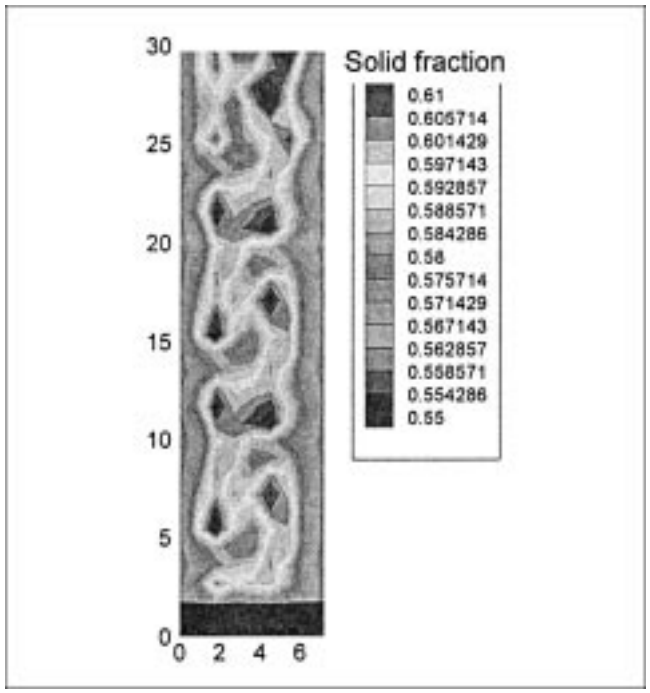

Figure 9. Solid holdup (THE1 = 1.0-bed porosity) distribution in the model trickle bed.

Note: lighter areas indicate higher bed porosity or bed voidage.

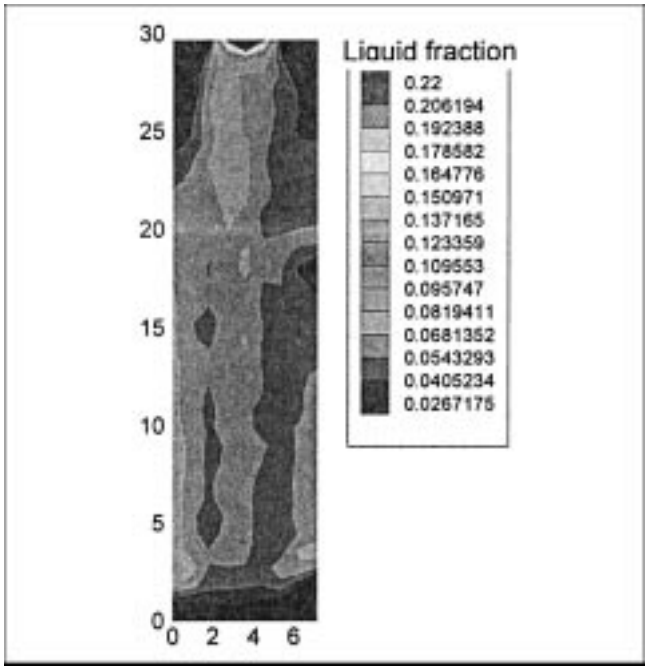

Figure 10. Steady-state liquid holdup (THE2) contours.

Note: lighter areas indicate higher liquid holdup.

The liquid flow distribution observed in the just-mentioned steady-state case was compared with transient simulations carried out with a liquid flow ON time of 15 s and a total cycle time of 60 s (45 s liquid OFF). Snapshots of the liquid flow distribution were taken at several time intervals ($t = 15$, 25, 40, 55 s from the beginning of liquid ON time) to compare them with the steady-state liquid holdup data obtained in the earlier simulation of the steady-state case. Contour plots of liquid holdup at $t = 15$, 25, 40, and 55 s are respectively shown in Figures 11a, 11b, 11c, and 11d. Liquid holdup variation over the reactor cross section is also depicted at several axial locations at different times in a typical flow modulation cycle (Figures 12a–12g). These figures clearly demonstrate that unsteady-state operation ensures better uniformity in liquid distribution at all locations over that observed in steady-state operation. This improved uniformity, although not perfect, does ensure enhanced liquid supply to all locations not previously possible during steady state (in particular, the bottom zones shown in Figures 11a and 11b). Figure 12 clearly shows that induced flow modulation results in better liquid spreading and even distribution of liquid over the entire cross section at each axial location at some point in time in the cycle. This also indicates that, although the average liquid holdup at each location may not exceed the steady-state holdup, the reactor performance may still be en-

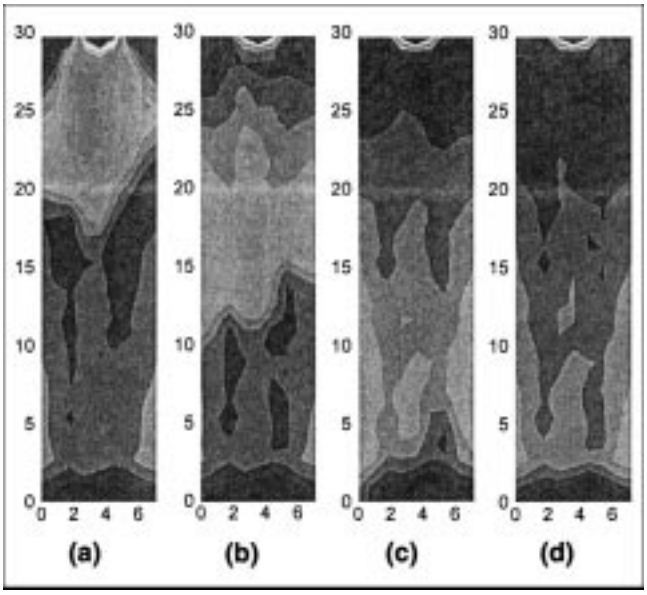

Figure 11. Liquid holdup (THE2) contours at different hues from start of the liquid ON cycle (left).

(a) $t = 15$ s; (b) $t = 25$ s; (c) $t = 40$ s; (d) $t = 55$ s. *Note:* lighter areas indicate higher liquid holdup.

hanced due to the higher than steady-state holdup for a subinterval of the entire cycle. This time interval of enhanced liquid supply can allow exchange of liquid reactants and products with the stagnant liquid and with the catalyst pellets present in any particular zone. Another observation that can be made from Figure 12 is that for some time interval, all zones in the reactor become almost completely devoid of liquid, and can allow enhanced access of the gaseous reactant to externally dry catalyst during this time interval. Temperature rise and internal drying of catalyst and faster gas-phase reaction may also occur in this interval, to be quenched by the liquid in the next cycle. This demonstrates the possibility of controlled rate enhancement due to induced flow modulation. It also facilitates our understanding and visualization of the phenomena occurring in the reactor. It confirms the reasons behind higher unsteady-state performance observed experimentally and simulated in the reaction transport 1-D model (Khadilkar et al., 1999). Incorporation of this type of CFD simulation into 2-D and 3-D reaction transport models will help more realistically and accurately quantify the observed enhancement.

Applications of Two-Fluid Model in Catalytic Packed Beds

There are a number of challenging issues to be solved in scale-up and scale-down of multiphase flow packed beds during process development. Particle size, for example, is one of the important parameters in the scale-up and scale-down of packed-bed processes because of its effects on the relative importance on particle wetting, axial dispersion, and the wall effect. As estimated by Sie and Krishna (1998), for a typical liquid in trickle-flow hydrotreating (kinematic viscosity $= 3 \times 10^{-7}$ m^2/s), an extrudate catalyst of 1.5-mm diameter can be safely tested in the pilot-plant reactor without apparent liquid maldistribution, but the bench scale as well as the microflow reactors are only suitable for testing smaller catalyst particles, such as 0.8 and 0.2 mm, respectively. Since the relations of bed structures, flow textures, and operating conditions vary with the changes of particle size and reactor scales, it is essential to have models that can forecast the changes in reactor performance while varying the reactor size. We show that one can utilize the *k*-fluid CFD model to obtain the main characteristics of the flow distribution in packed-bed reactors, and to develop a quantitative relation of bed structure and flow distribution. In the next step of reactor performance simulation, one should adopt the cell-network model concept in which the flow-field information from *k*-fluid CFD simulation can be applied. By doing this, the complex kinetics can be efficiently incorporated into the multiphase flow modeling results, which should provide a good alternative for modeling of multiphase reactive flows in packed beds.

Scaling up

The industrial design procedure for multiphase packed-bed reactors still relies on empiricism. The desired capacity and conversion required determines the total catalyst volume. Taking into account the total amount of heat generated (for example) and the specific heats of the process streams as well as the maximum allowed temperature rise per bed, the number of beds, the distribution of catalyst over the beds, and the quench gas flows are determined. The reactor models used for design are mostly plug flow, axial dispersion, or cells in series. These models are not able to capture the reactor performance when the flow patterns are a far departure from those ideal cases. These models also cannot provide reliable diagnostic service for the operating units, which is mostly required due to flow maldistribution (Jaffe, 1976). The bed parameters normally used in modeling are particle size, shape factor, bed porosity, and bed dimensions without any attention paid to porosity distribution and velocity distribution. Sims et al. (1994) found that better predictions of the reactor performance could be obtained when considering the liquid velocity variation in a two-region cell model than when using a plug-flow assumption. In this work, we devise a new paradigm in which both variations of structure and flow are taken into account in reactor modeling. The left column in Figure 13 displays the conventional design parameters, and the right column displays the new design approach. In the new procedure, instead of only considering the mean design quantities, one considers the mean quantities plus the variance of these quantities. It is expected that such a design methodology should provide the mean and variance for the reactor performance. This design scheme should be able to provide comprehensive information on species conversion contours and selectivity contours in the whole domain of the packed-bed reactor, which is needed for the diagnostic analysis of the operating reactors. Beyond the numerous hydrodynamics correlations, one needs to have quantitative relations on the distributions involved. In other words, one needs to develop a set of correlations for the distributed quantities, as shown in Figure 13.

The developed *k*-fluid CFD model, together with the experimental measurements with MRI, can accomplish the pre-

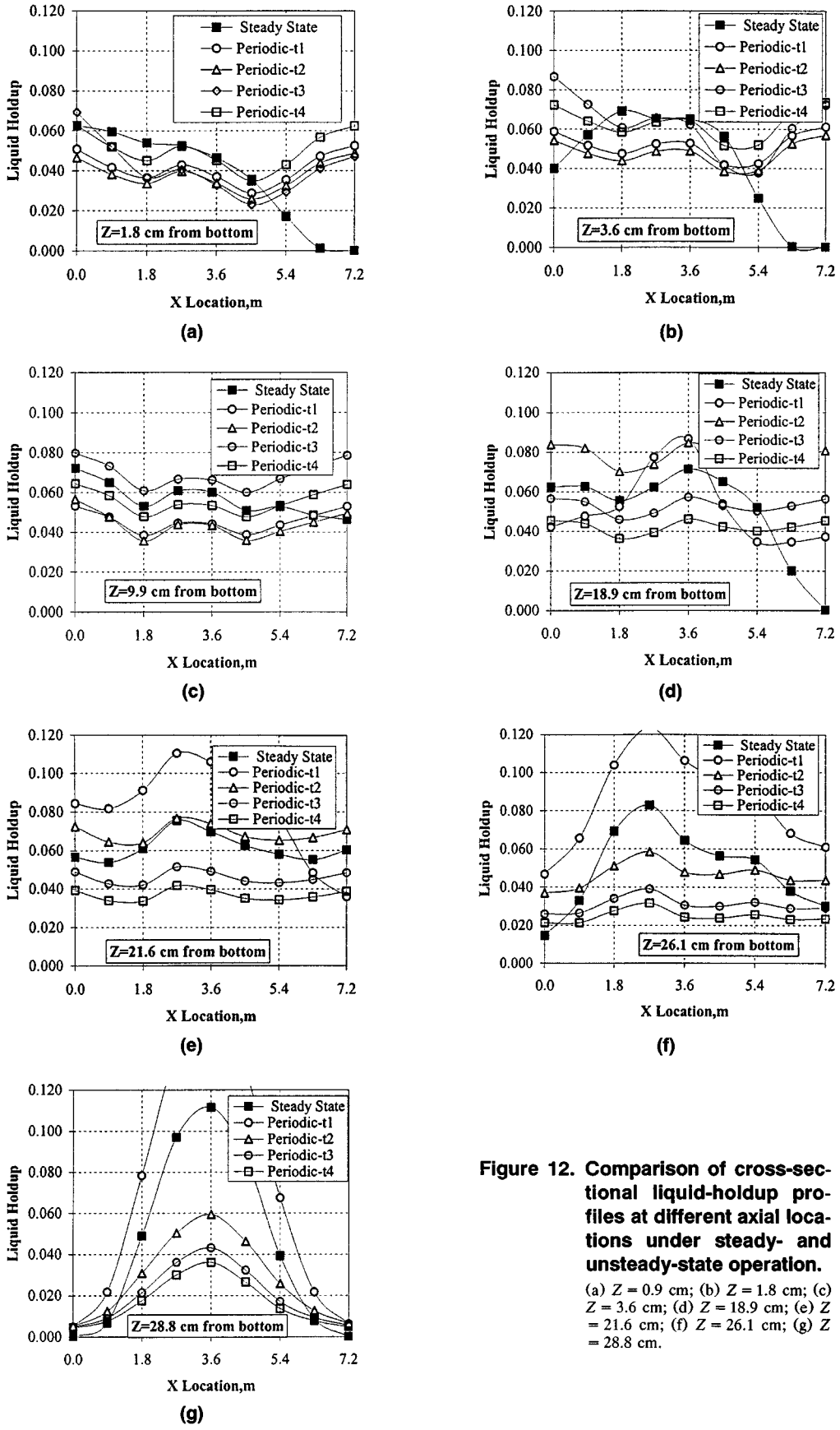

Figure 12. Comparison of cross-sectional liquid-holdup profiles at different axial locations under steady- and unsteady-state operation.

(a) $Z = 0.9$ cm; (b) $Z = 1.8$ cm; (c) $Z = 3.6$ cm; (d) $Z = 18.9$ cm; (e) $Z = 21.6$ cm; (f) $Z = 26.1$ cm; (g) $Z = 28.8$ cm.

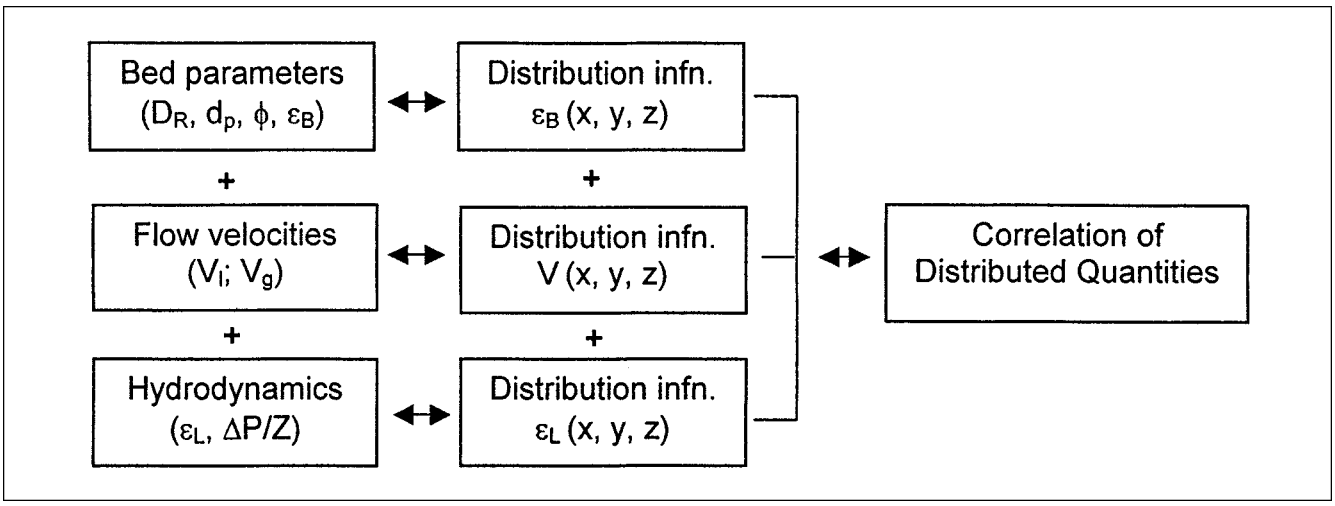

Figure 13. New design procedure for packed-bed reactors.

ceding task. The preliminary simulation efforts of using the CFD two-fluid model in quantifying the relationship between bed structure and macroscale flow were reported elsewhere for gas–liquid cocurrent downflow in trickle beds (Jiang et al., 2001a), and CFD was shown to be an efficient numerical tool for doing this. On the experimental side, Sederman et al. (1998) probed the structure-flow correlations within the interstitial space of a packed bed with liquid upflow using MRI volume- and velocity-measurement techniques. Such techniques can be extended to packed beds with multiphase flow, and to quantify structure-flow correlations and validate CFD modeling results. Additional discussion of the new paradigm for reactor modeling and design is available in Jiang (2000).

Scaling down

Flow maldistribution in either a bench-scale or commercial-scale packed bed is often responsible for the failure of the scaled-down unit to mimic the performance of the large reactor. The modeling of multiphase flow in the bench-scale unit is needed for proper interpretation of reaction-rate data obtained in such units. Understanding the mechanism of flow maldistribution is the first step to avoiding it. In order to achieve this objective, the *k*-fluid CFD model is applied to simulate the two-phase flow distribution in a bench-scale cylindrical tube (e.g., 1-in. diameter) packed with small-size catalyst particles (e.g., 1.5 mm). A detailed discussion of this application is available elsewhere (Jiang et al., 2001b), a set of typical simulation results is given in this subsection to demonstrate the capability of the developed model in developing the understanding of the flow distribution in bench-scale catalytic packed beds.

Figure 14a shows the input solid volume fraction (THE1) distribution used in the CFD *k*-fluid model of a 1-in. packed bed at liquid superficial velocity of 0.05 cm/s and gas superficial velocity of 6.0 cm/s. The gas and liquid physical properties are those typical of hydrotreating reaction. The following values are selected for densities, $\rho_l = 0.652$ g/cm^3, $\rho_g =$ 0.00187 g/cm^3, and for kinematic viscosities of liquid: 0.0014 cm^2/s, and gas: 0.0809 cm^2/s. The simulated liquid holdup maldistribution and pressure distribution are respectively shown in Figures 14b and 14c. Clearly, at low liquid velocity, partial particle wetting occurs, which results in a significant contribution of capillary pressure to the liquid holdup distribution. Liquid more likely stays in the low-porosity zones. The opposite trend of the liquid holdup distribution can be expected due to the fully wetted particles at high liquid superficial velocity: higher porosity zones correspond to higher liquid holdup, as discussed in Jiang et al. (2001a). The single-point pressure measurement is known to often give scattered results when the packing is repacked. Even for fixed

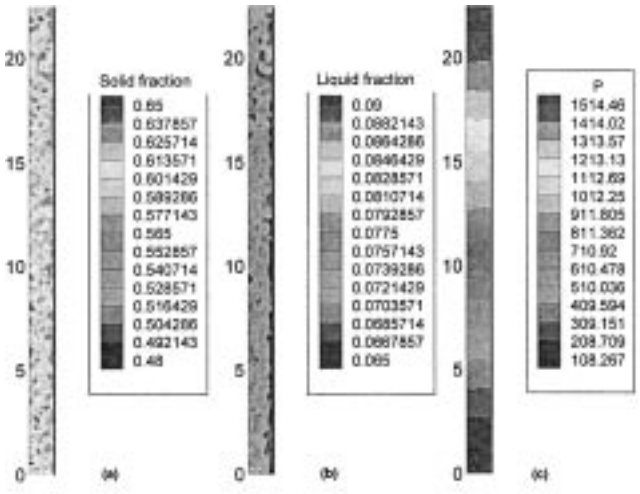

Figure 14. Input solid volume-fraction distribution and simulated liquid-holdup distribution and pressure distribution from two-fluid CFD model in 1-in. diameter packed bed with particle size of 1.5 mm.

(a) Solid volume-fraction (THE1); (b) liquid holdup (THE2); (c) pressure (in dyn/cm^2). Flow conditions: $U_{l0} =$ 0.05 cm/s, $U_{g0} = 6.0$ cm/s.

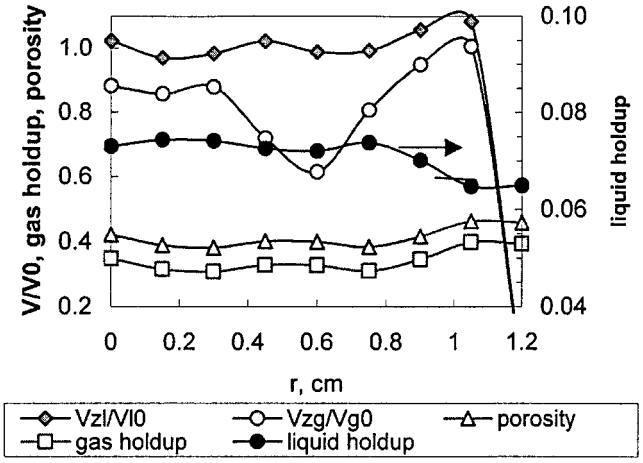

Figure 15a. Relative interstitial velocity profiles of gas and liquid phase, volume fraction profiles of porosity, gas, and liquid in the radial direction at low flow rates.

$U_{l0} = 0.05$ cm/s; $U_{g0} = 6.0$ cm/s.

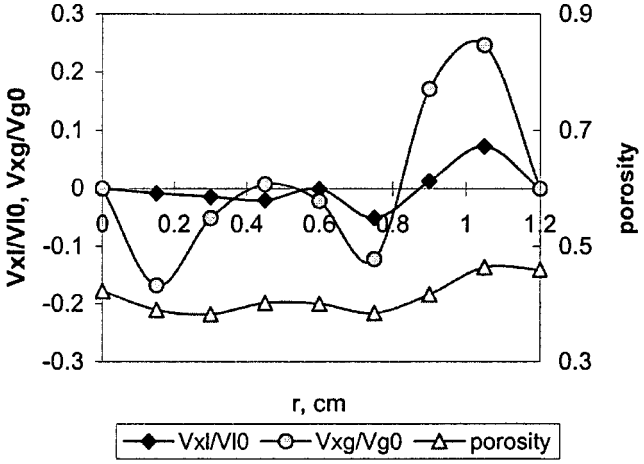

Figure 16a. Relative interstitial velocity profiles of gas and liquid phase, porosity profiles in the radial direction at low flow rates.

$U_{l0} = 0.05$ cm/s; $U_{g0} = 6.0$ cm/s.

packing the radial profile of pressure does exist, as shown in Figure 14c.

The capability of the model in predicting maldistribution is further illustrated in Figures 15a and 15b, which display the simulated longitudinal-averaged velocity profiles of the axial and horizontal velocity components (V_z and V_x) for gas and liquid flows at relatively low gas and liquid superficial velocities ($U_{l0} = 0.05$ cm/s, $U_{g0} = 6.0$ cm/s). Figures 16a and 16b display the corresponding results at relatively high gas and liquid velocities ($U_{l0} = 1.0$ cm/s, $U_{g0} = 12.0$ cm/s). Figure 17 shows the frequency plots of each sectional relative interstitial velocity (V/V_0) at both low and high flow conditions. More uniform two-phase flow distribution is observed at the high flow rates, and more nonuniform gas flow is found when the liquid superficial velocity is low ($U_{l0} = 0.05$ cm/s). Particle partial wetting causes more nonuniform interstitial space left for gas flow.

Conclusions

Comparison of the *k*-fluid CFD simulation and the experimental results has been performed for both liquid upflow and gas–liquid cocurrent downflow in packed beds. The effects of feed-flow distributions have been simulated for bench-scale and pilot-scale packed beds at steady-state and unsteady-state flow conditions. The applications of the *k*-fluid model in the scaling up and scaling down of packed beds have been discussed. The following conclusions are reached:

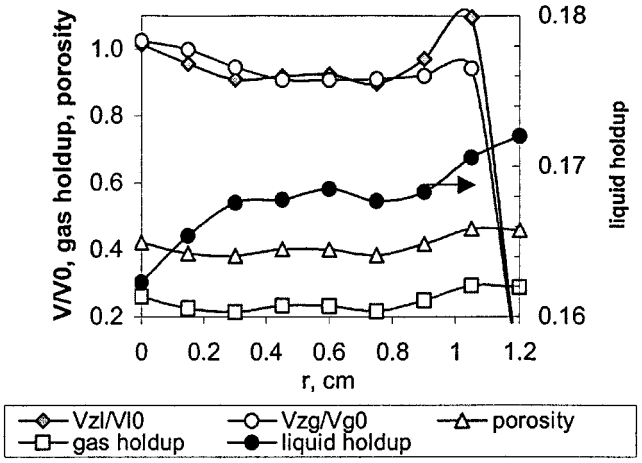

Figure 15b. Relative interstitial velocity profiles of gas and liquid phase, volume fraction profiles of porosity, gas, and liquid in the radial direction at low flow rates.

$U_{l0} = 1.0$ cm/s; $U_{g0} = 12.0$ cm/s.

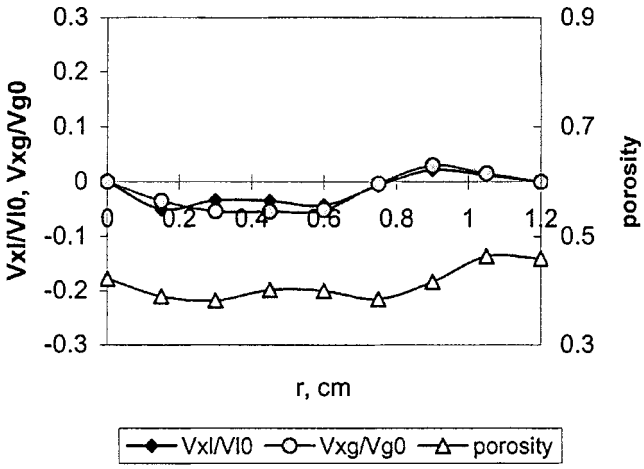

Figure 16b. Relative interstitial velocity profiles of gas and liquid phase, porosity profile in the radial direction at low flow rates.

$U_{l0} = 1.0$ cm/s; $U_{g0} = 12.0$ cm/s.

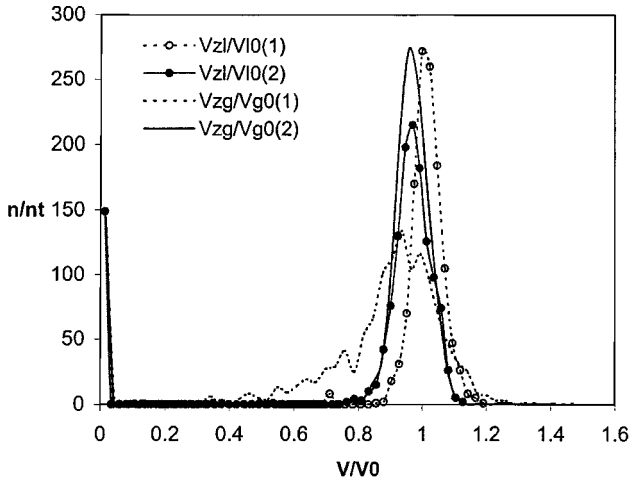

Figure 17. Relative interstitial velocities of gas and liquid phase at low (1: $U_{l0} = 0.05$ cm/s; $U_{g0} = 6.0$ cm/s) and high (2: $U_{l0} = 1.0$ cm/s; $U_{g0} = 12.0$ cm/s) flow rates.

n/nt = a fraction of section number in the total section number.

1. The *k*-fluid CFD model can capture the longitudinally averaged radial profile of axial liquid velocity and the probability density function of the sectional velocity, provided that the following information is available: (i) mean porosity, (ii) longitudinally averaged radial porosity profile, and (iii) sectional porosity distribution type and its variance.

2. For a gas–liquid cocurrent down-flow system, the predictions of the *k*-fluid CFD model of the global liquid saturation and pressure gradient are comparable with the experimental data in Szady and Sundaresan (1991) and with the predictions of suitable phenomenological models.

3. The *k*-fluid model can simulate the dynamic flow pattern under periodic inflow condition, which ensures better uniformity in liquid distribution at all locations over that observed in steady-state operation.

4. One can establish the structure–flow relationship using the *k*-fluid CFD model. Such a relationship is helpful for the scale-up and scale-down of packed beds. The *k*-fluid CFD model can also provide detailed flow information for the mixing-cell network model to evaluate the performance of packed-bed reactors.

Additional studies are needed in (1) experimental validation of closures and benchmark cases, and (2) better estimation of structural information using MRI data for 2-D and 3-D beds.

Acknowledgments

We gratefully acknowledge the support of CREL industrial sponsors that made this work possible, and thank the Los Alamos National Laboratory for providing the CFDLIB code. Special thanks are due to Dr. S. Kumar and Dr. S. Roy for valuable discussions of many CFD issues.

Notation

d_p = diameter of particle, m
D_r = diameter of column, m
H = length of packed bed, m
P = pressure, pa
l_s = section size, m
r = radial position, m or cm
Re_p = particle Reynolds number
t = time, s
THE1, 2, 3 = solid, liquid, and gas volume fraction
U_g = gas superficial velocity, m/s
U_{g0} = gas-feed superficial velocity, m/s
U_l = liquid superficial velocity, m/s
U_{l0} = liquid-feed superficial velocity, m/s
V_g = gas interstitial velocity, m/s
V_{g0} = gas-feed interstitial velocity ($= U_{l0}/\epsilon_B$), m/s
V_l = liquid interstitial velocity, m/s
V_{l0} = liquid-feed interstitial velocity ($= U_{g0}/\epsilon_B$), m/s
V_x = interstitial velocity component in horizontal or radial direction, m/s
V_z = interstitial velocity component in axial direction, cm/s
Z = axial position, cm or m

Greek letters

ϵ_g = gas holdup
ϵ_l = liquid holdup
ϵ_l^0 = static liquid holdup
ϕ = particle shape factor (for sphere, $\phi = 1.0$)
ρ_g = density of gas phase, kg/m^3
ρ_l = density of liquid phase, kg/m^3
φ = angular coordinate

Literature Cited

Al Dahhan, M. M., and M. P. Dudukovic, "Catalyst Wetting Ethancy in Trickle-Bed Reactors at High Pressure," *Chem. Eng. Sci.*, **50**, 2377 (1995).

Anderson, D. H., and A. V. Sapre, "Trickle Bed Reactor Flow Simulation," *AIChE J.*, **37**, 377 (1991).

Attou, A., C. Boyer, and G. Ferschneider, "Modeling the Hydrodynamics of the Cocurrent Gas-Liquid Trickle Flow through a Trickle-Bed Reactor," *Chem. Eng. Sci.*, **54**, 785 (1999).

Baldwin, C. A., A. Sederman, M. D. Mantle, P. Alexander, and L. F. Gladden, "Determination and Characterization of the Structure of a Pore Space from 3D Volume Images," *J. Colloid Interface Sci.*, **181**, 79 (1996).

Benenati, R. F., and C. B. Brosilow, "Void Fraction Distribution in Beds of Spheres," *AIChE J.*, **8**, 359 (1962).

Bey, O., and G. Eigenberger, "Fluid Flow Through Catalyst Filled Tubes, *Chem. Eng. Sci.*, **52**, 1365 (1997).

Boelhouwer, J. G., H. W. Piepers, and B. H. H. Drinkenburg, "The Induction of Pulse in Trickle-Bed Reactors by Cycling the Liquid Feed," *Chem. Sci. Eng.*, **56**, 2605 (2001).

Christensen, G., S. J. McGovern, and S. Sundaresan, "Cocurrent Downflow of Air and Water in a Two-Dimensional Packed Columns," *AIChE J.*, **32**, 1677 (1986).

Deans, H. A., and L. Lapidus, "A Computational Model for Predicting and Correlating the Behavior of Fixed-Bed Reactors: 1. Derivation of Model for Nonreactive Systems," *AIChE J.*, **6**, 656 (1960).

Haure, D. A., R. R. Hudgins, and P. L. Silveston, "Periodic Operation of a Trickle-Bed Reactor," *AIChE J.*, **35**, 1437 (1989).

Holub, R. A., M. P. Dudukovic, and P. A. Ramachandran, "A Phenomenological Model for Pressure Drop, Liquid Holdup, and Flow Regime Transition in Gas-Liquid Trickle Flow," *Chem. Eng. Sci.*, **47**, 2343 (1992).

Jaffe, S. B., "Hot Spot Simulation in Commercial Hydrogenation Processes," *Ind. Eng. Chem. Res.*, **15**, 410 (1976).

Jiang, Y., M. R., Khadilkar, M. H. Al-Dahhan, and M. P. Dudukovic, "Two-Phase Flow Distribution in 2D Trickle-Bed Reactors," *Chem. Eng. Sci.*, **54**, 2409 (1999).

Jiang, Y., "Flow Distribution and its Impact on Performance of Packed-Bed Reactors," PhD Diss., Washington Univ., St. Louis, MO (2000).

Jiang, Y., M. R. Khadilkar, M. H. Al-Dahhan, and M. P. Dudukovic, "Single Phase Flow Modeling in Packed Beds: Discrete Cell Approach Revisited," *Chem. Eng. Sci.*, **55**, 1829 (2000).
Jiang, Y., M. H. Al-Dahhan, and M. P. Dudukovic, "Statistical Characterization of Macroscale Multiphase Flow Textures in Trickle Beds," *Chem. Eng. Sci.*, **56**, 1647 (2001a).
Jiang, Y., M. R. Khadilkar, M. H. Al-Dahhan, and M. P. Dudukovic, "CFD Modeling of Multiphase Flow Distribution in Catalytic Packed-Bed Reactors: Scale Down Issues," *Catal. Today*, **66**, 209 (2001b).
Jiang, Y., M. R. Khadilkar, M. H. Al-Dahhan, and M. P. Dudukovic, "CFD of Multiphase Flow in Packed-Bed Reactors I. *k*-Fluid Modeling Issues," *AIChE J.*, **48**(4), 701 (2002).
Johnson, N. L., "The Legacy and Future of CFD at Los Alamos," Canadian CFD Conference, Ottawa, Canada (1996).
Johnson, N. L., B. A. Kashiwa, and W. B. Vander Heyden, "Multiphase Flows and Particle Methods (Part-B)," Annual Conference of the Computational Fluid Dynamics Society of Canada, British Columbia, Canada (1997).
Kashiwa, B. A., N. T. Padial, R. M. Rauenzahn, and W. B. Vander Heyden, ASME Symp. on Numerical Methods for Multiphase Flows, Lake Tahoe, Nevada (1994).
Khadilkar, M. R., M. H. Al-Dahhan, and M. P. Dudukovic, "Parameter Study of Unsteady State Flow Modulation in Trickle Bed Reactors," *Chem. Eng. Sci.*, **54**, 2585 (1999).
Kuipers, J. A. M., and W. P. M. van Swaaij, "Computational Fluid Dynamics Applied to Chemical Reaction Engineering," *Advances in Chemical Engineering*, Vol. **24**, J. Wei et al., eds., Academic Press, San Diego, CA, p. 227 (1998).
Lahey, R. T., Jr., and D. A. Drew, "The Analysis of Two-Phase Flow and Heat Transfer Using a Multidimensional, Four Field, Two-Fluid Model," *NURETH-9*, San Francisco, CA (1999).
Manz, B., L. F. Gladden, and P. B. Warren, "Flow and Dispersion in Porous Media: Lattice-Boltzmann and NMR Studies," *AIChE J.*, **45**, 1845 (1999).
Mears, D. E., "The Role of Axial Dispersion in Trickle-Flow Laboratory Reactor," *Chem. Eng. Sci.*, **26**, 1361 (1971).
Moller, L. B., C. Halken, J. A. Hansen, and J. Bartholdy, "Liquid and Gas Distribution in Trickle-Bed Reactors," *Ind. Eng. Chem. Res.*, **35**, 926 (1996).
Mueller, G. E., "Prediction of Radial Porosity Distribution in Randomly Packed Fixed Beds of Uniformly Sized Spheres in Cylindrical Containers," *Chem. Eng. Sci.*, **46**, 706 (1991).
Pan, Y., M. P. Dudukovic, and M. Cheng, "Numerical Investigation of Gas-Driven Flow in 2-D Bubble Columns," *AIChE J.*, **46**, 434 (2000).
Saez, A. E., and R. G. Carbonell, "Hydrodynamic Parameters for Gas-Liquid Cocurrent Flow in Packed Beds," *AIChE J.*, **31**, 52 (1985).
Sederman, A. J., M. L. Johns, A. S. Bramley, P. Alexander, and L. F. Gladden, "Magnetic Resonance Imaging of Liquid Flow and Pore Structure within Packed Beds," *Chem. Eng. Sci.*, **52**, 2239 (1997).
Sederman, A. J., M. L. Johns, P. Alexander, and L. F. Gladden, "Structure-Flow Correlations in Packed Beds," *Chem. Eng. Sci.*, **53**, 2117 (1998).
Sie, S. T., and R. Krishna, "Process Development and Scale Up: III. Scale-Up and Scale-Down of Trickle Bed Processes," *Rev. Chem. Eng.*, **14**, 203 (1998).
Silveston, P. L., "New Applications of Periodic Operations," *Unsteady State Processes Catalyst*, Yu. Su. Matros, ed., VSP Zeist, Utrecht, The Netherlands, p. 217 (1990).
Sims, B. W., S. W. Gaskey, and D. Luss, "Effect of Flow Regime and Liquid Velocity on Conversion in Trickle-Bed Reactor," *Ind. Eng. Chem. Res.*, **33**, 2530 (1994).
Stanek, V., *Fixed Bed Operations: Flow Distribution and Efficiency*, Ellis Horwood Series in Chem. Eng., Ellis Horwood, New York (1994).
Stephenson, J. L., and W. E. Stewart, "Optical Measurements of Porosity Distribution of a Single-Phase Fluid Flowing in Packed Beds," *Chem. Eng. Sci.*, **53**, 1375 (1986).
Szady, M. J., and S. Sundaresan, "Effect of Boundaries on Trickle-Bed Hydrodynamics," *AIChE J.*, **37**, 1237 (1991).
Tasmatsoulis, D., and N. Papayannakos, "Simulation of Non-Ideal Flow in a Trickle Bed Reactors by a Cross-Flow Model," *Chem. Eng. Sci.*, **50**, 3685 (1995).
Tory, E. M., B. H. Church, M. K. Tam, and M. Ratner, "Simulated Random Packing of Equal Spheres," *Can. J. Chem. Eng.*, **51**, 484 (1973).
Tsochatzidis, N. A., and A. J. Karabelas, "Properties of Pulsing Flow in a Trickle Bed," *AIChE J.*, **41**, 2371 (1995).
Yin, F. H., C. G. Sun, A. Afacan, K. Nandakumar, and K. T. Chung, "CFD Modeling of Mass-Transfer Processes in Randomly Packed Distillation Columns," *Ind. Eng. Chem. Res.*, **39**, 1369 (2000).

Manuscript received Mar. 23, 2001, and revision received Sept. 10, 2001.